LIMNOLOGY
and
OCEANOGRAPHY: METHODS

Limnol. Oceanogr.: Methods 4, 2006, 227–236

Assessment of submarine groundwater discharge by handheld aerial infrared imagery: case study of Kaloko fishpond and bay, Hawai'i

T. Ka'eo Duarte,[1] Harold F. Hemond,[2] Donald Frankel,[3] and Sheila Frankel[2]
[1]Water Resources Research Center, University of Hawai'i at Mânoa, Honolulu, HI, USA
[2]Parsons Lab, CEE, Massachusetts Institute of Technology, Cambridge, MA, USA
[3]Lincoln Lab, Massachusetts Institute of Technology, Lexington, MA, USA

Abstract

Handheld aerial infrared imagery was used to infer submarine groundwater discharge (SGD) to a Hawaiian fishpond and adjacent bay at Kaloko, Hawai'i, using heat as a tracer for the relatively cooler groundwater. Use of a handheld infrared camera aboard readily available, unmodified aircraft is a convenient and less expensive alternative to use of a camera mounted in the belly of a customized aircraft, although it favors taking images with an oblique view instead of the preferable nadir view. Pond-wide patterns of SGD were readily apparent in oblique images and were typically more apparent in infrared imagery than in ground truth data, due to the formation of thin (order of cm) surface strata of groundwater which could easily fail to be observed with conventional temperature probes. Absolute temperature measurement is affected by the variation of surface emissivity and reflectivity with angle of camera view; corrections based on use of Fresnel's equation were of the order of several degrees centigrade at convenient oblique aerial viewing angles. Other factors that may affect apparent water temperature include sky temperature and camera error. Surface waves may also account for variations in average surface emissivity and reflectance that were not accounted for by the aforementioned corrections. Under suitable conditions, handheld aerial infrared imagery revealed spatial patterns of groundwater inflow, detected differences in water temperature at the meter scale, and measured absolute water temperature with accuracy on the order of 2 to 3 °C.

Introduction

Understanding the locations and rates of coastal submarine groundwater discharge (SGD) is necessary to better define the coastal boundary condition and mixing dynamics in coastal aquifer models and to characterize the transport of nutrients and contaminants to the marine environment. Adequate characterization is difficult, however, because of the large areas involved and the spatial and temporal variability of flow. SGD is usually assessed via (1) modeling, (2) direct measurement, or (3) tracer techniques (Burnett et al. 2002, Burnett et al. 2001, Oberdorfer 2003).

The modeling approach takes the form of either water budgets over a specified watershed area (Destouni and Prieto 2003, Kaneshiro and Peterson 1977, Smith and Nield 2003, Young et al. 1977) or models of actual groundwater flow in porous media via Darcy's law (Li et al. 1999, Robinson and Gallagher 1999, Smith and Zawadzki 2003, Uchiyama et al. 2000). These models are primarily useful to estimate average SGD over large areas and give little to no resolution of spatial heterogeneity in seepage.

Seepage meters may be employed to better understand SGD flux patterns on smaller scales and to quantify localized discharge volumes and associated contaminant or nutrient concentrations (Bokuniewicz 1980, Burnett et al. 2002, Cable et al. 1997, Charette et al. 2001, Garrison et al. 2003, Kim et al. 2003, Michael et al. 2003, Portney et al. 1998, Sholkovitz et al. 2003, Smith and Zawadzki 2003, Taniguchi et al. 2003). However, seepage meters are labor intensive, problematic when flows are small (Belanger and Montgomery 1992, Shinn et al. 2002), and unsuitable for installation on steep, rocky, heterogeneous, and rough coastlines as exist at our study site.

Geochemical tracers can provide information on the percentage of SGD in parcels of seawater (Garrison et al. 2003, Kim et al. 2003, Moore 1999, Uchiyama et al. 2000). Isotopic tracers, such as ^{226}Ra, ^{222}Rn, $\delta^{18}O$, and δD, necessitate point water sampling and lab analyses. Salinity measurements have

Acknowledgments

We thank Sallie Beavers and other staff of Kaloko-Honokohau National Historical Park (permit KAHO-2003-SCI-0004), students participating in the 2003, 2004, and 2005 TREX program of MIT's department of Civil and Environmental Engineering, the Northeast Educational Foundation, and the W. H. Leonhard chair held by H.F.H. for financial, logistical, and field assistance.

the advantage that in situ measurements may often be made with adequate accuracy and precision for their purpose. In both instances, groundwater and marine water composition must be known, and a suitable average composition must be assumed in cases where the composition fluctuates with time or location on the upland watershed.

Heat can also be used as a tracer by exploiting the temperature difference between groundwater and coastal water. This method is analogous to the use of salinity in that it requires assumptions about the temperatures of both a groundwater end member and a coastal marine end member. This method is most applicable where a large temperature difference exists, and where the effects of other sources of heat (e.g., solar heating, flow of sensible or latent heat) can be ignored or corrections can be applied.

Use of temperature has the particular advantage that it can be measured rapidly over large areas by remote thermal infrared (IR) imaging (Banks et al. 1996, Lavery et al. 1993, Torgersen et al. 2001). In Hawai'i, infrared and multispectral imaging of the coastlines were conducted as early as the late 1960s (Adams and Lepley 1968, Fischer et al. 1966, Lepley and Palmer 1967); however, little ground truthing was conducted. Infrared technology has advanced greatly in the last 30 years, and handheld infrared cameras are now accessible to many researchers. In this article, we explore a method using such cameras to rapidly map SGD by measuring surface water temperature over large areas of water in a coastal Hawaiian fishpond.

A light aircraft is an attractive camera platform from the standpoint of cost relative to the areal coverage possible. A disadvantage is that, unless modified with a belly window, such aircraft are only convenient for obtaining oblique views. Oblique views will require correction for 2 effects as a function of viewing angle. First, the water's emissivity is reduced by an amount equal to its reflectivity. Second, reflected radiation will also reach the detector. As the angle of incidence increases, the reflectivity increases nonlinearly. In the measurements presented here, the water surface reflectivity is substantial, and the reflected source is usually cloud-free sky, which is at a noticeably lower temperature than the water.

Fresnel first derived the relationship between incident radiant power and the reflected and refracted power at the boundary between different dielectric media. The result can be derived from Maxwell's equations (see, for example, Marion 1965). For radiation polarized perpendicular to the plane of incidence, the reflection coefficient is

$$R_{\perp} = \frac{\sin^2(\theta_2 - \theta_0)}{\sin^2(\theta_2 + \theta_0)},$$

where θ_0 and θ_2 are the angles of incidence and refraction, respectively. For parallel polarization, the result is

$$R_{par} = \frac{\tan^2(\theta_2 - \theta_0)}{\tan^2(\theta_2 + \theta_0)}.$$

Reflectivity for any other polarization is a linear combination of these two. We assumed random polarization, and thus used a value of R equal to the average of $R_{\perp}$ and R_{par}. θ_0 is related to θ_2 by Snell's law,

$$\frac{n_2}{n_0} = \frac{\sin(\theta_0)}{\sin(\theta_2)}.$$

Corrections for the angle of observation have been made by other investigators. Eagleson (1970) indicated that reflectivity of a water surface under clear sky conditions is satisfactorily described by Fresnel's formula. Sugihara et al. (1993) measured surface temperature of Uchiura Bay using oblique views from a land-mounted thermal IR radiometer operating in the 7 to 9 μm range and were able to obtain good fits to temperatures measured from a ship after applying corrections for emissivity and reflectance based on Fresnel's formula.

In this work, we used a handheld imaging radiometer (FLIR camera), viewing scenes at oblique angles from the passenger-side window of a light plane, to measure both (1) relative temperature distribution in the pond, as an indicator of the presence and pattern of SGD, and (2) absolute surface temperature. To provide data needed to calculate viewing angle corrections, we developed a practical technique to determine the constantly changing viewing angle from the aircraft. We also tested viewing angle corrections by taking IR images of a small artificial play pool, using a goniometer to measure camera angle. Ground-based measurements of temperature and salinity in the fishpond provided absolute temperature information as well as confirmation of temperature as a valid tracer for groundwater inflow. The surface-based measurements also yielded information on temperature and salinity layering within the water column and the implications of this layering on the interpretation of aerial IR data in such ponds.

Materials and procedures

FLIR aerial infrared imagery—Aerial imagery was obtained using a model TVS-700 handheld thermal imaging radiometer during January 2003 and January 2004. Images were obtained through the open right-side window of a Cessna 172 Skyhawk, a single-engine, 4-seat, high-wing aircraft. To permit the window to open fully, a licensed mechanic removed the one screw that fastens this window to a restraint bracket. When the bracket is disconnected and the window is opened during normal flight and with flaps retracted, aerodynamic forces lift the window up flat against the underside of the wing. The aircraft is approved for flight with the window fully open.

Orbits were flown around Kaloko fishpond and environs at approximately 38 m/s (85 mph) and 300 m (1000 feet) above the surface, or slightly lower as cleared by air traffic control. To create a navigational record from which the camera position and viewing angle could be calculated, a handheld Garmin Gecko GPS receiver was carried aboard during the flights in January 2004 and was programmed to record position in 3 dimensions every 10 s. To provide the GPS unit with an adequate view of satellites, it was taped to nylon cord and suspended between cargo tie points directly beneath the rear win-

dow of the aircraft. Afterward, position data were downloaded to a spreadsheet program and matched to infrared images by comparing (with interpolation if necessary) the GPS position timestamps with the image timestamps.

To provide reference locations for surface truth measurements, small buoys were temporarily placed in Kaloko and surveyed using a Trimble Pro XRS GPS. Buoys were located on each aerial image by the following procedure: (i) vertical angle and azimuth angle between each buoy and the camera were calculated trigonometrically using aircraft and buoy latitude, longitude, and altitude data, (ii) digital photographs were taken of a map on which each buoy location had been marked, using the same oblique camera angle and azimuth angle for the digital camera as was calculated for the aerial FLIR camera, (iii) the digital images were printed onto vu-graph transparencies at convenient scales that matched the infrared images as portrayed on a computer screen, and (iv) buoy locations were transferred onto the oblique infrared images by overlaying the images.

Artificial pool experiments—To provide a water surface whose temperature could be controlled and measured readily, a children's play pool was set up on shore and filled with water from Kaloko fishpond. Thermal imagery of the pool surface was obtained from a stepladder at several viewing angles using the same TVS-700 handheld thermal imaging radiometer that was used for aerial work. Angle of view from the vertical was measured to the nearest degree by mounting the camera on a goniometer, built from a carpenter's protractor that incorporated a built-in plumb needle. Three Hydrolab mini-sondes were established along the edges of the pool to continuously measure temperature. The pool was in a location sheltered from wind, but waves could be produced on the water surface by flexing the pool edges.

Estimation of surface water temperatures from FLIR imagery—For 2004 aerial and play pool data only, files representing infrared images were displayed using Thermonitor software, and at each location of interest, apparent temperature was read using an emissivity of 1.0 and averaging over the order of 100 pixels. Groups of pixels were designated on the IR images, by eye, at locations where ground truth data were available, and pixels were averaged using the box tool provided in the Thermonitor software. Single pixels corresponded to dimensions from 1 to 3 m in the aerial data and approximately 1 cm in the play pool data. Groups of approximately 100 pixels corresponded to 10 to 30 m in the aerial data and approximately 10 cm in the play pool data. Apparent temperatures were not sensitive to the exact number of pixels in the averaging area, rarely differing by more than 0.1 or 0.2 °C among repeated selections of groups of pixels from the same image.

Temperature corrections were calculated as a function of viewing angle, which in most aerial images ranged between 50 and 70 degrees from the vertical. First, apparent temperatures at an emissivity of 1.0 were used to calculate total radiance of the water surface at each point. Reflectance was calculated from Fresnel's law, and our best estimate of actual emissivity was then calculated as (1.0 – reflectance). The contribution of sky reflection to observed total radiance was calculated as the product of reflectance and an estimated average sky radiance. Several values of sky radiance were used; the sensitivity of the results to assumed sky temperature is discussed in the section below on absolute water temperatures.

Surface survey of pond—Temperature and salinity measurements of the water column of Kaloko fishpond were made during January 2003, 2004, and 2005 by undergraduate student workers from aboard kayaks. Sampling locations were fixed by reference to the aforementioned buoys, to maps drawn by the workers, or to GPS coordinates. To avoid loss of salinity and temperature gradients by inadvertent mixing, it was necessary to use a minimum amount of paddling when moving to a sampling location. The preferred technique was to coast into a sampling area using only wind drift or a kayak's momentum. Measurements were made using the conductivity and temperature sensors of Hydrolab minisonde probes in 2003 and part of 2004. On January 21, 2004, and in 2005, high-resolution measurements were taken within the upper few centimeters of water. Temperature was measured with high resolution using hand-held digital temperature probes (DeltaTRAK Professional) whose active sensing areas corresponded to the distal few millimeters of a metal probe. High-spatial-resolution salinity measurements were taken using 1-mL graduated plastic pipettes, lowered to the desired depth while preventing inflow by blocking the upper end with a finger. At the desired depth, pipettes were vented to allow sample inflow, then again blocked while being withdrawn from the pond. Samples of approximately 0.1 mL were placed on the window of a Bausch and Lomb model 366 handheld salinity refractometer. The readability of the refractometer was between 0.5 and 1 ppT.

Assessment

Study site—Kaloko fishpond and bay are located in Kaloko-Honokohau National Historical Park along the western coastline of Hawai'i island, Hawai'i (Figure 1). Hawaiian fishponds (*loko i'a*) such as Kaloko were an important part of Hawaiian culture and food production. Although largely in disuse today, these low-energy, slightly human-modified estuaries may be found along coastlines throughout the Hawaiian archipelago and provide favorable conditions for evaluating the use of thermal IR for detecting coastal seepage.

The highly permeable basalts of both a'a and pahoehoe types at Kaloko are associated with Hualalai volcano. Due to the young age of the lava flows, little to no soil cover exists over much of the area, and vegetation is sparse. The coastline is very rocky with occasional sand beach areas. The reef off of Kaloko is young and limited in extent. Because there are no surface water streams in the area, all rainfall that is not evapotranspired or pumped by wells discharges to the ocean via the basal lens. The coastal basal lens has a fairly thick fresh-to-saline transition zone, and, with the possible exception of localized high-discharge areas, the discharging water is brack-

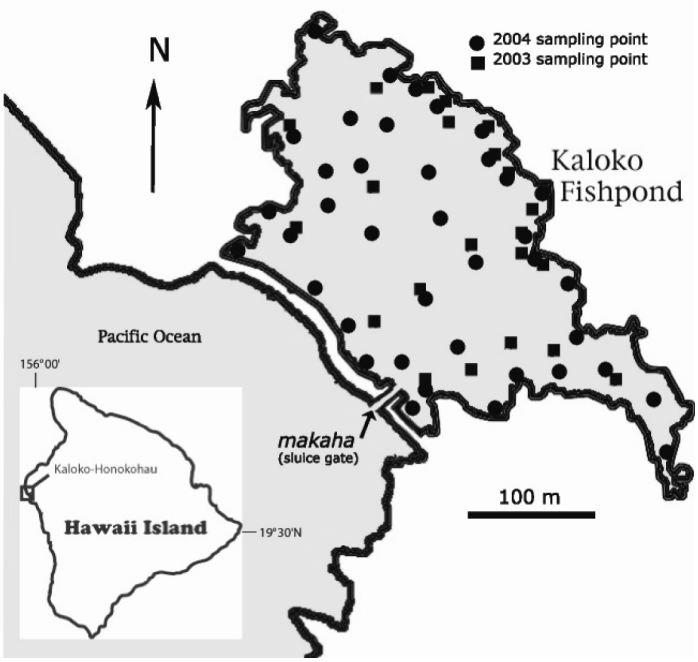

Fig. 1. Kaloko Fishpond and Bay with surface survey sampling points from January 2003 and January 2004. The *makaha*, or sluice gates, provide controlled pond-ocean connections in Hawaiian fishponds and aid in cycling of water, nutrients, and fish.

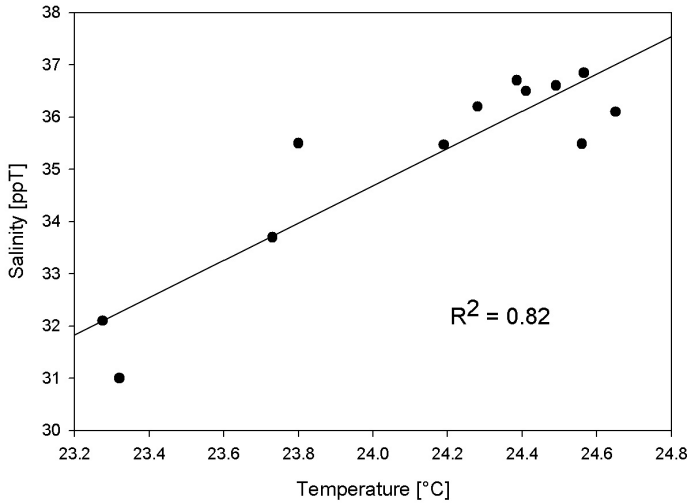

Fig. 2. Salinity correlation with temperature for the eastern border of Kaloko fishpond. Salinity readings taken from top of water column with Hydrolab probe on 01/18/2003 between 1033 and 1108 HST.

ish rather than fresh (Oki et al. 1999). Young et al. (1977) estimated "probable" SGD at 6.4 million gallons a day per mile (mgd/mile) of coastline, Kaneshiro and Peterson (1977) gave a value of 6.38 mgd/mile, and Oki (1999) estimated 3 mgd/mile. The above studies did not attempt to characterize coastal groundwater discharge patterns.

Temperature as a predictor of SGD—We assumed that the salinity of water samples from Kaloko Pond provided, through use of a conservative mixing model, a direct measure of the proportion of SGD-derived water that they contained. Because the discharging water is brackish, the SGD end member of this mixing model has salinity that is a significant fraction of the salinity of seawater. To test the hypothesis that temperature could also provide a useful measure of SGD, we examined the relationship between temperature and salinity data obtained using the Hydrolab probes. These data should be well correlated, assuming SGD and seawater temperatures are each sufficiently uniform, and if sources of heat other than those embodied by SGD and seawater are small enough that they can be neglected.

The expected significant positive correlation could be found, especially early in the day (Figure 2). Lower temperatures correlated with lower salinities, both being lower in groundwater than in seawater at this location and time. Density differences driven by salinity at this site are larger than, and in opposition to, those driven by temperature. Solar heating effects visibly degraded this relationship. For example, measurements of temperature and salinity made along the eastern boundary of the pond between 1033 and 1108 local time on 01/18/03 were correlated with R^2 = 0.82, whereas among all data obtained in the pond between 1007 and 1527 on the same day R^2 was only 0.17. The highest temperature observed in the earlier data set was 24.6 °C, whereas the highest temperature in the latter set was 26 °C, corresponding to a temperature rise of the same order of magnitude as the sought-after SGD signal.

Patterns of surface temperature observed by FLIR—Knowing that lower temperatures in fact provided a useful surrogate measure of the presence of SGD, we expected that inflow areas could be visualized as relatively low-temperature areas by infrared imagery, perhaps even without observation angle corrections. FLIR images, taken as early as practicable in the day to minimize the confounding effects of solar heating, consistently showed the presence of relatively lower surface temperatures in the southeast corner and along the east shore of Kaloko fishpond in both 2003 and 2004 (Figure 3). This pattern was persistent from scene to scene, and was not dependent on either azimuth angle or vertical angle of observation. Interestingly, this pattern was not clear in the Hydrolab-derived temperature measurements, for reasons that became evident later when the cooler ground-derived water was found to be present as a thin stratified surface layer, which the relatively large Hydrolab probes could not resolve.

Close to the shore, the images suggested the presence of a very narrow band of warmer temperatures, which may be due to (1) a semiwetted perimeter of rocks/vegetation which would be cooler than dry rocks/vegetation yet warmer than the water; (2) the near-shore areas being areas of more rapid solar heating (due to absorbed energy being distributed over a smaller depth of water); or (3) reflectance of infrared energy from the near-shore vegetation (which is warmer than the sky).

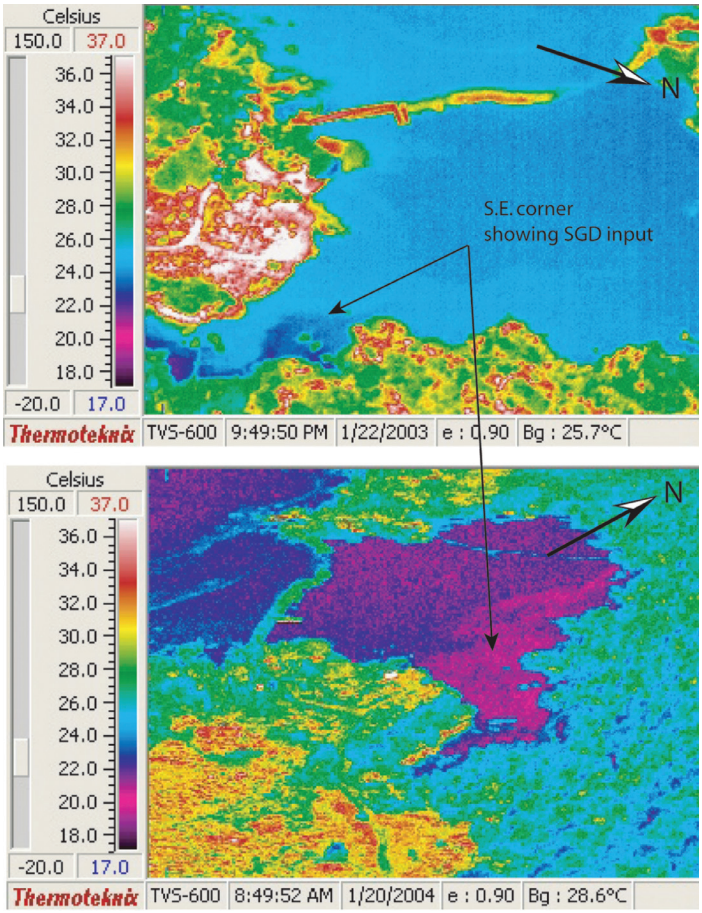

Fig. 3. FLIR images from 2003 (top) and 2004 (bottom) both showing cooler water along the southeastern edge of the pond.

The January 2004 image indicates a larger area of cooler surface water compared with January 2003. We do not have enough data to sufficiently explain this difference, but it may be due to differences in upland recharge conditions and/or tides and mixing conditions.

High-resolution temperature and salinity profiles—Suspecting that the differences between temperature patterns observed in the Hydrolab data and in the infrared images could be due to stratification on a small (centimeter) scale, we measured surface water temperature and salinity on 1/21/04 in the upper few centimeters of Kaloko fishpond using high-resolution techniques. Weather on 1/21/04 was very similar to that on 1/20/04, and measurements were taken at the same early time of day. Significant near-surface temperature and salinity gradients were observed in the areas shown as being cooler in the FLIR imagery, but not elsewhere, consistent with the presence of a surface layer of cooler, less-saline water. Figure 4 plots depth versus salinity and temperature at sampling buoy 21, which is representative of gradients seen in the southeast end of the pond. Temperature differences between near-surface water and deeper water were as high as 3 °C or slightly more. By contrast, the lowest surface salinity observed in the south-

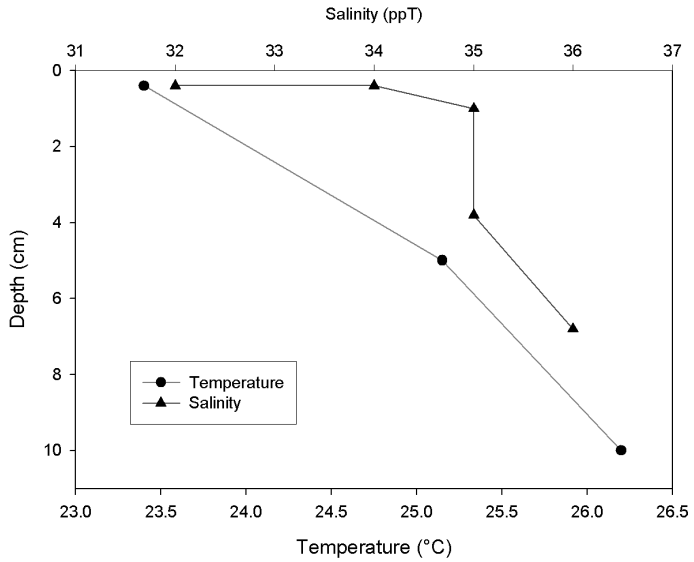

Fig. 4. Temperature and salinity stratification at a representative sampling point (buoy 21) in south-eastern area of the pond on 01/21/2004.

east area of the pond was 16 ppT, and all salinities at the deepest depth that could be accurately sampled using available pipettes (about 15 cm) equaled or exceeded 30 ppT; salinity was very close to 35 ppT elsewhere in Kaloko pond on this date. On both days, unusually high surf and wind conditions for the Kona coast prevailed, implying that stratification might be even stronger on a more typical, calm Kona day.

Similar results were observed in a more extensive high-resolution survey of temperature and salinity throughout the pond during January 2005 (Figure 5). Although there is considerable variation at shallow depths, which is expected given that some points have little SGD influence and some are

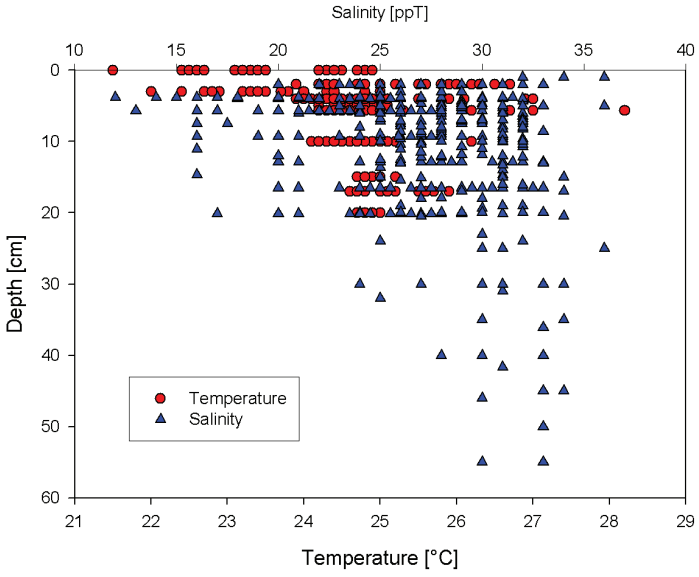

Fig. 5. Salinity versus depth throughout the entire of Kaloko fishpond on 01/15/2005 and 01/16/2005 between 1030 and 1600 HST.

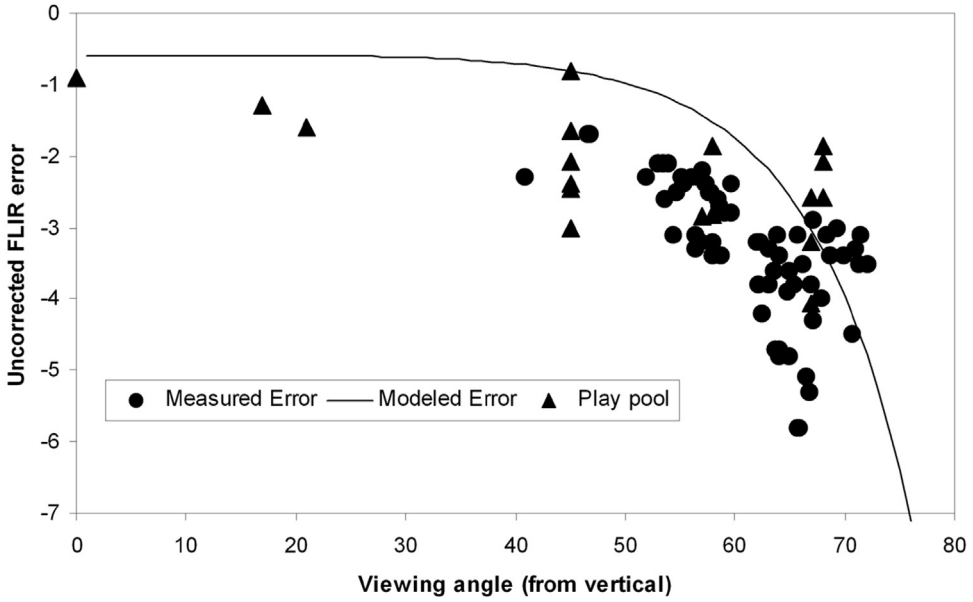

Fig. 6. Difference between uncorrected FLIR recorded temperatures and surface survey measurements plotted against FLIR camera viewing angle. Solid line represents the theoretical error that would arise in camera-inferred temperatures according to the Fresnel equation. Plot includes both aerial and play pond data from January 2004.

strongly influenced by SGD, it is evident that cooler, fresher water is restricted to the top tens of centimeters of the water column.

At certain locations, the interface between the cooler, less saline surface water and the underlying marine water layer could also be observed visually, mainly by refraction at the interface, but also by accumulation of small pieces of detritus in the interface region. It is noteworthy, also, that we did not observe stratification using the Hydrolab probes, either owing to their large dimensions relative to the stratified structure or to mixing induced by inserting the larger probes into the water.

Absolute water temperature values inferred from FLIR—Detailed comparison of FLIR and bulk water temperatures were made for a series of 3 images, all taken in the vicinity of 0900 local time on 20 Jan 2004. These images were chosen for their good framing of the entire pond, close spacing in time early in the day, relatively high density of surface-based measurements taken at nearly the same time, and availability of GPS navigational data. We excluded stations that were located where we had observed evidence of SGD spreading out on the surface, based either on a pattern of cooler surface temperatures in FLIR imagery or on microscale sampling. This was intended to eliminate from the analysis those sites where distinct stratification was likely to be present on a several-centimeters scale. At the submillimeter scale, a temperature gradient is expected to exist within a surface film at all sites, causing the temperature inferred from infrared radiance to underestimate bulk water temperature even without the intrusion of SGD. Fewer acceptable surface measurements were available for comparison with FLIR measurements later in the morning because the rate of water warming from insolation increased relative to the rate at which surface crews could make complete rounds of the pond.

Temperature measurements taken from the upper water column with Hydrolab probes averaged 25.3 ± 0.3 °C. Uncorrected FLIR temperatures using an emissivity of unity were lower, ranging from 21.6 to 22.4 °C in image no. 67, 20.7 to 22.4 °C in image no. 71, and 19.6 to 21.8 °C in image no. 75. On average, the apparent temperature measured by FLIR using an emissivity of unity was at least 3 °C lower than the ground-based measurements, and error was greatest for the largest observation angles. For individual locations viewed at large (order of 75 degrees) angles from the vertical, the error was as large as 5 to 6 °C. Mean temperature error would be about 2° less if the assumptions of a water surface emissivity of 0.97, and no sky reflectance, were made. Total error may include both an error in estimating the temperature of the radiating, uppermost film of water and a difference between the temperature of this film and the temperature at the Hydrolab probe depth, as explained in the previous section.

In FLIR observations of the artificial play pool, a similar pattern was observed. Although fewer data points were obtained, the range of observation angles exceeded that of the aerial images and ranged from 68 to 0 degrees. The largest temperature error observed was 4°; in all cases FLIR-derived temperatures were lower than those measured in situ. The differences between uncorrected FLIR-inferred temperatures and temperatures measured by Hydrolab probes are shown as a function of observation angle, for both the pond and the artificial pool, in Figure 6. In this plot, the magnitude of error that should theoretically result from decreased emissivity at non-

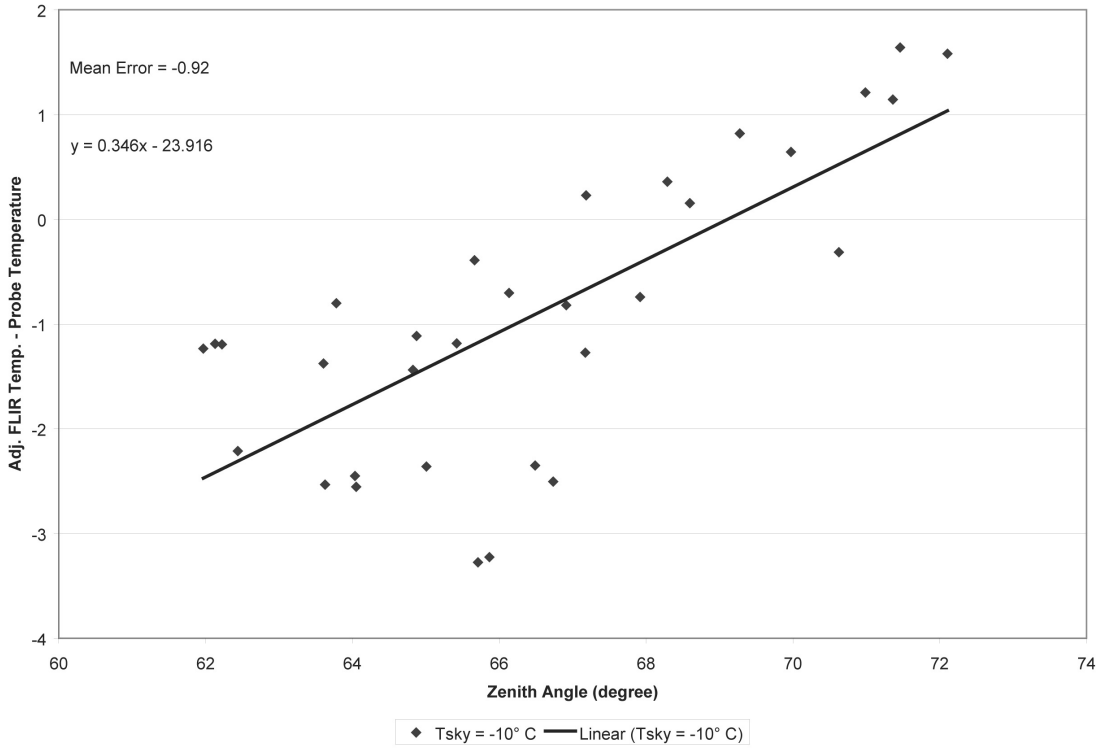

Fig. 7. Difference between corrected FLIR recorded temperatures and surface survey measurements plotted against FLIR camera viewing angle. Plot includes both aerial and play pond data from January 2004.

vertical observation angles, as calculated from the Fresnel equation, is shown as a solid line.

Fortunately, the search for patterns of colder water indicating SGD will not be affected much by the change in angle of observation. At a given angle of observation, the emissivity and reflectivity are affected equally regardless of the surface or sky temperature, so any patterns of low temperature will persist. Of course, in the limit of grazing incidence (angle of observation approaching 90 degrees), the FLIR image will be dominated by radiation from the sky, but this geometry amounts to observing the horizon, which is easily avoided. At worst, a gradient of temperature across the entire image in the direction of the plane of incidence could be expected. Since the FLIR camera field of view in the vertical dimension is about 19 degrees, the reflectivity of the water surface for a centerline viewing angle of 60 degrees will increase from about 5% at the bottom of the image to about 15% near the top. A change of this magnitude, spread across the entire water surface, is unlikely to obscure temperature patterns produced by different water parcels in the image.

Application of corrections using reasonable estimates of sky temperature resulted in closer agreement between FLIR and ground survey temperatures. However, because we did not systematically take sky images, sky temperatures were poorly constrained, and our correction must also assume that sky temperature is invariant with azimuth angle and altitude. Correction based on a sky temperature of –10 °C resulted in an average value (corrected FLIR temperature – measured water temperature) ranging from +0.8 °C for image no. 67 (in which most of the image was at angles exceeding 65 degrees from the vertical and many points were at viewing angles exceeding 70 degrees), to –2.4 °C for image no. 75 (in which more than half of the points were at angles of less than 65 degrees). There was thus a trend of overcorrection at higher viewing angles, a trend that was also observed when these corrections were applied to the play pool observations (Figure 7).

One possible reason for overcorrection at high angles may be that the sky temperature we used was too low. Although this possibility is reinforced by our limited observation of apparent sky temperatures (in the vicinity of +20 °C near the horizon), the use of a high enough sky temperature in the correction algorithm to eliminate the overcorrection trend at high angles (a temperature of about 20 °C) resulted in average corrected FLIR temperatures being systematically low by the order of 4 °C (Figure 8).

Some underestimation of water temperature is expected owing to heat loss by evaporation at the water surface, because IR imagery senses radiation from only an uppermost submillimeter-thick skin of the water body. Emery et al. (1994) indicated that this effect can exceed 1 °C in the ocean, but is typically of the order of 0.5 °C. This effect is thus unlikely to explain all of the observed bias. Nor is bulk stratification in

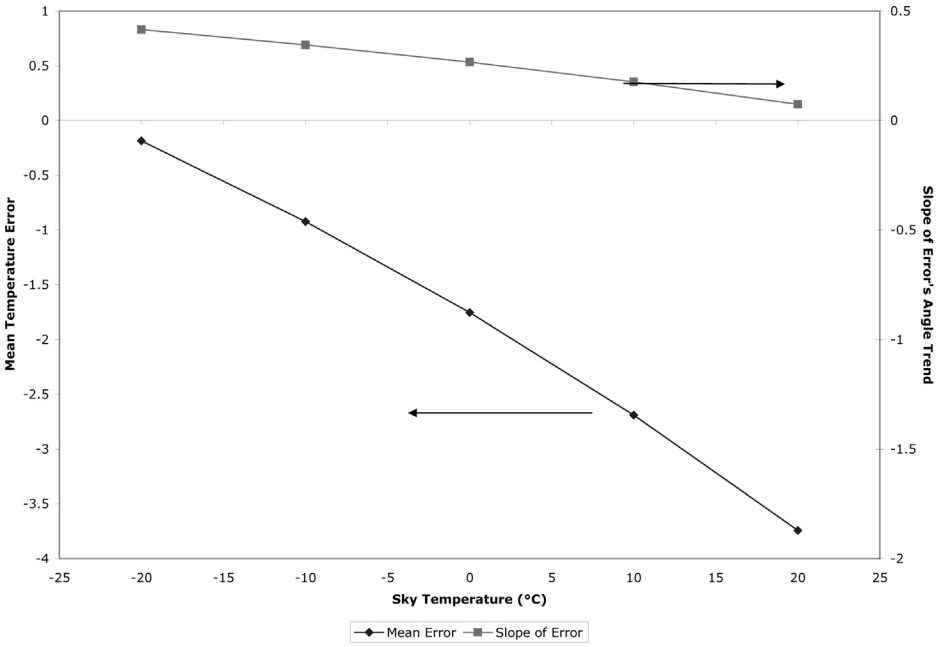

Fig. 8. Mean FLIR temperature error and mean dependence of FLIR temperature on viewing angle determined for the Kaloko data set as a function of the sky temperature used in the viewing angle correction.

the pond likely to explain this difference; the points shown in Figures 6 and 7 were from the play pool and from parts of the fishpond where stratification appeared to be absent.

Absorbance by the atmosphere over the imaging path would create a negative bias on temperature. However, Sugihara et al. (1993) found that errors in temperature due to path attenuation were not significant in their field experiments, except perhaps at very large angles (> 70 degrees).

Another potential source of bias in absolute temperature as measured by FLIR is the camera. Friedman and Flug (2003) measured absolute error of a TVS-700 by recording single exposures to a black body plate held at a series of known temperatures, and found that bias trended downward as the temperature rose, ranging from +4.8 to –5.4 °C over the range of 0 to 60 °C. This bias observed by these workers was less than +0.8°, however, when the plate temperature was held between 20 and 25 °C. The authors did not develop a formal correction to the absolute temperature because temperature differences were more important to their purpose. It is not known how these values of bias may vary among cameras, or as a function of time in a single camera. It may also be possible for temperature gradients within the camera, perhaps exacerbated by holding the camera in the aircraft's slipstream, to contribute to error.

Bias in absolute temperature measurements such as found by Friedman and Flug (2003) affects the absolute temperature measurement. It will have little effect on the ability to find patterns of lower temperature surface water, because detecting patterns of SGD depends on differential temperature measurement. The camera performs an internal flat-field calibration either at regular intervals or when the camera's internal temperature changes by more than a small amount since the previous calibration. During flat-field calibration, a uniform temperature flat plate is placed in front of the optics. The gain and offset of each detector element is then adjusted so that the response is uniform across the array. Using single exposures, Friedman and Flug (2003) found that the bias for differential measurement was 0.3 °C and was independent of temperature. They attributed all apparent non-uniformity in bias across the focal plane to non-uniformities in the blackbody source.

Camera bias may be the source of the behavior of the viewing angle correction described above and shown in Figure 8. An assumed sky temperature that minimizes the surface temperature error averaged over all viewing angles has a trend in error as a function of viewing angle. An assumed sky temperature for which the error is largely independent of the viewing angle has a greater than minimum average error. This angle-independent error may be camera bias.

It is also possible that a specular reflection model based on the Fresnel equation and the assumption of a flat water surface is overly simple, and that the geometry of ripples and waves has a measurable effect on bulk reflectance and emissivity. Although we have no quantitative or systematic measures of the wave field at Kaloko fishpond during our experiments (it was minimal but present, with amplitudes of perhaps 10 cm at most), if this effect were important then a systematic role of azimuth angle on sky reflection would be expected in the case of a uniform wave field. We examined incidental FLIR observations of the ocean surface adjacent to Kaloko pond at a wide range of azimuth angles and observed no systematic variation in apparent ocean temperature, how-

ever. We also measured temperature of the play pool with and without the generation of O(1 cm) surface waves and observed only small (< 1 °C) effects. Sugihara et al. (1993) obtained good corrections for observation angle without invoking surface wave effects.

Discussion

Observation of surface temperature *patterns* using oblique FLIR imagery proved very useful for revealing the pond-wide distribution of SGD. Use of FLIR imagery not only involved much less labor than ground-based measurements, but also proved more sensitive to the presence of groundwater, mainly because the lower-temperature groundwater was in many locations thinly layered over seawater.

Measurement of absolute surface temperature at Kaloko by means of FLIR imagery had significant errors of both bias and scatter. Corrections based on Fresnel's formula decreased but did not eliminate bias, which could in principle arise from several independent mechanisms including non-uniform sky temperatures, surface ripple effects, and camera-related effects.

The magnitude of error sources found in IR observations of Kaloko are also likely to be present in previous IR studies conducted in Hawaii (Adams and Lepley 1968, Fischer et al. 1966, Lepley and Palmer 1967). Further, since these studies look at open coastlines, in which wave breaking likely presents additional effects on IR emission from the surface, it is possible that many locations of "cool water" in their images may not in fact indicate areas of higher SGD. Informal aerial IR observations that we made along the western coast of Hawai'i incidental to the Kaloko study suggest that white foam associated with wave breaking looks systematically cooler than surrounding water when viewed in thermal IR images. Because this pattern appeared in all images, whereas SGD is likely heterogeneous, we speculate that such foam areas may look cooler due to lower emissivity or microscale cooling effects on bubble surfaces.

Comments and recommendations

In the course of field and aerial surveys at Kaloko a number of practical suggestions arose. As also found by Torgersen et al. (2001) and Banks et al. (1996), minimizing the confounding effects of solar heating can be important to successful IR surveying. For the tropical Pacific, where groundwater is cooler than the near-shore waters and solar heating is often severe, morning surveys are recommended.

Correction for viewing angle is necessary if absolute temperatures are to be estimated with the greatest possible accuracy from oblique views. To obtain the data necessary to calculate viewing angle, continuous logging of aircraft position by GPS proved to be very successful. Direct measurement of apparent sky temperature distribution should be done in future surveys. A practical means of making such measurements is to take images of the sky at a series of camera elevation angles, ranging from the horizon to the zenith, using a simple goniometer to estimate angle. The camera should view the desired aquatic scenes at an angle as nearly straight down as possible, by a combination of banking the plane over the target area and angling the camera downward as far as practicable, consistent with seeing the viewfinder and resisting wind forces. Simultaneously taking FLIR and visible digital video images, as done by Torgersen et al. (2001), may be useful if results may be affected by land cover, e.g., vegetation type and extent.

Ground truth for calibration purposes is essential and requires temperature and salinity measurements. Where stratification is possible, we recommend that surface observations be made with subcentimeter vertical resolution, inasmuch as probes having poorer spatial resolution may fail to identify the presence of thin surface layers derived from groundwater inflow. It should be noted, however, that when the stratified layers are thick or when more strongly mixed conditions occur, larger probes can successfully map SGD, as has been found at He'eia Fishpond on the island of O'ahu (T.K.D., unpublished data).

Handheld infrared imagery is most suitable for delineation of SGD when

- there are clear temperature differences between seawater and the discharging groundwater,
- the water body has low enough wave action that the SGD is not immediately mixed, and
- measurements are taken when solar heating effects are low

References

Adams, W. M., and L. K. Lepley. 1968. Infrared images of the Ka'u and Puna coastlines on Hawaii. 26, Water Resources Research Center, Honolulu.

Banks, W. S. L., R. L. Paylor, and W. B. Hughes. 1996. Using thermal-infrared imagery to delineate groundwater discharge. Groundwater 24:434-443.

Belanger, T. V., and M. T. Montgomery. 1992. Seepage meter errors. Estuarine Coastal Marine Sci. 10:437-444.

Bokuniewicz, H. J. 1980. Groundwater seepage into Great South Bay, New York. Estuarine Coastal Marine Sci. 10: 437-444.

Burnett, B., and others. 2002. Assessing methodologies for measuring groundwater discharge to the ocean. EOS 83: 117-122.

Burnett, W. C., M. Taniguchi, and J. Oberdorfer. 2001. Measurement and significance of the direct discharge of groundwater into the coastal zone. J. Sea Res. 46:109-116.

Cable, J. E., W. C. Burnett, and J. P. Chanton. 1997. Magnitude and variations of groundwater seepage along a Florida marine shoreline. Biogeochemistry 38:189-205.

Charette, M. A., K. O. Buesseler, and J. E. Andrews. 2001. Utility of radium isotopes for evaluating the input and transport of groundwater-derived nitrogen to a Cape Cod estuary. Limnol. Oceanogr. 46:465-470.

Destouni, G., and C. Prieto. 2003. On the possibility for generic modeling of submarine groundwater discharge. Biogeochemistry 66:171-186.

Eagleson, P. S. 1970. Dynamic Hydrology. McGraw-Hill, New York.

Emery, W. J., Y. Yu, G. A. Wick, P. Schlussel, and R. W. Reynolds. 1994. Correcting infrared satellite estimates of sea surface temperature for atmospheric water vapor attenuation. J. Geophys. Res. 99:5219-5236.

Fischer, W. A., D. A. Davis, and T. M. Sousa. 1966. Fresh water springs of Hawaii from infrared images. *In*: U.S. Geological Survey hydrology atlas. U.S. Geological Survey.

Friedman, M., and E. Flug. 2003. Differential and absolute temperature calibration of a thermal imaging radiometer. U.S. Army Night Vision and Electronic Sensors Directorate, Fort Belvoir, VA, USA.

Garrison, G. H., C. R. Glenn, and G. M. McMurtry. 2003. Measurement of submarine groundwater discharge in Kahana Bay, Oahu, Hawaii. Limnol. Oceanogr 48:920-928.

Kaneshiro, B. Y., and F. L. Peterson. 1977. Groundwater recharge and coastal discharge for the northwest coast of the island of Hawaii: a computerized water budget approach. 110, Water Resources Research Center, Honolulu.

Kim, G., K.-K. Lee, K.-S. Park, D.-W. Hwang, and H.-S. Yang. 2003. Large submarine groundwater discharge (SGD) from a volcanic island. Geophys. Res. Lett. 30(21), Article No. 2098.

Lavery, P., C. Pattiaratchi, A. Wyllie, and P. Hick. 1993. Water quality monitoring in estuarine water using the Landsat thematic mapper. Remote Sens. Environ. 46:268-280.

Lepley, L. K., and L. A. Palmer. 1967. Remote sensing of Hawaiian coastal springs using multispectral and infrared imaging. 18, Water Resources Research Center, Honolulu.

Li, L., D. A. Barry, F. Stagnitti, and J.-Y. Parlange. 1999. Submarine groundwater discharge and associated chemical input to a coastal sea. Water Resources Res. 35:3253-3259.

Marion, Jerry B. 1965. Classical Electromagnetic Radiation, Academic Press, NY, p. 163-166.

Michael, H. A., J. S. Lubetsky, and C. F. Harvey. 2003. Characterizing submarine groundwater discharge: a seepage meter study in Waquoit Bay, Massachusetts. Geophys. Res. Lett. 30(6), Article No. 1297.

Moore, W. S. 1999. The subterranean estuary: a reaction zone of groundwater and seawater. Marine Chem. 65:111-125.

Oberdorfer, J. 2003. Hydrogeologic modeling of submarine groundwater discharge: comparison to other quantitative methods. Biogeochemistry 66:159-169.

Oki, D. S., G. W. Tribble, W. R. Souza, and E. L. Bolke. 1999. Ground-water resources in Kaloko-Honokohau National Historic Park, Island of Hawaii, and numerical simulation of the effects of ground-water withdrawals. 99-4070, U.S. Geological Survey, Honolulu.

Portnoy, J. W., B. L. Nowicki, C. T. Roman, and D. W. Urish. 1998. The discharge of nitrate-contaminated groundwater from developed shoreline to marsh-fringed estuary. Water Resources Res. 34:3095-3104.

Robinson, M. A., and D. L. Gallagher. 1999. A model of ground water discharge from an unconfined aquifer. Groundwater 37:80-87.

Shinn, E. A., C. D. Reich, and T. D. Hickey. 2002. Seepage meters and Bernoulli's revenge. Estuaries 25:126-132.

Sholkovitz, E., C. Herbold, and M. A. Charette. 2003. An automated dye-dilution based seepage meter for time-series measurement of submarine groundwater discharge. Limnol. Oceanogr. Methods 1:16-28.

Smith, A. J., and S. P. Nield. 2003. Groundwater discharge from the superficial aquifer into Cockburn Sound Western Australia: estimation by inshore water balance. Biogeochemistry 66:125-144.

Smith, L., and W. Zawadzki. 2003. A hydrogeologic model of submarine groundwater discharge: Florida intercomparison experiment. Biogeochemistry 66:95-110.

Sugihara, S., T. Ishiyama, and T. Yoshimura. 1993. Angular correction of sea surface temperature observed by thermal infrared radiometer. Int. J. Remote Sensing 14: 1339-1346

Taniguchi, M., J. V. Turner, and A. Smith. 2003. Evaluations of groundwater discharge rates from subsurface temperature in Cockburn Sound, Western Australia. Biogeochemistry 66:111-124.

Torgersen, C. E., R. N. Faux, B. A. McIntosh, N. J. Poage, and D. J. Norton. 2001. Airborne thermal remote sensing for water temperature assessment in rivers and streams. Remote Sens. Environ. 76:386-398.

Uchiyama, Y., K. Nadaoka, P. Rolke, K. Adachi, and H. Yagi. 2000. Submarine groundwater discharge into the sea and associated nutrient transport in a sandy beach. Water Resources Res. 36:1467-1479.

Young, R. H. F., A. E. Kay, L. S. Lau, E. D. Stroup, S. J. Dollar, and D. P. Fellows. 1977. Hydrologic and ecologic inventories of the coastal waters of west Hawaii. 105, NOAA Sea Grant, Honolulu.

Submitted 15 April 2005
Revised 28 October 2005
Accepted 6 April 2006